CHEMISTRY
A European Journal

Supporting Information

Derivation of Lanthanide Series Crystal Field Parameters From First Principles

Julie Jung,[a] M. Ashraful Islam,[b] Vincent L. Pecoraro,[c] Talal Mallah,[d] Claude Berthon,[e] and Hélène Bolvin*[b]

chem_201903141_sm_miscellaneous_information.pdf

Author Contributions

H.B. Conceptualization: Lead; Methodology: Lead; Project Administration: Lead; Writing - Original Draft: Lead; Calculations: Lead
J.J. Methodology: Equal; Writing - Original Draft: Equal; Calculations: Equal
M.I. Writing - Review & Editing: Supporting; Calculations: Supporting
V.P. Writing - Review & Editing: Supporting; Supply of Experimental Data: Equal
T.M. Writing - Review & Editing: Supporting; Supply of Experimental Data: Supporting
C.B. Supply of Experimental Data: Equal.

Derivation of Lanthanide Series Crystal Field Parameters From First Principles. Supplementary Information

Julie Jung[a], Md. Ashraful Islam[b], Vincent L. Pecoraro[c], Talal Mallah[d], Claude Berthon[e], Hélène Bolvin [b f *]

Contents

[a]Theoretical division, Los Alamos National Laboratory, Los Alamos, New Mexico 87545, USA.

[b]Laboratoire de Chimie et Physique Quantiques, CNRS, Université Toulouse III, 118 route de Narbonne, 31062 Toulouse, France.

[c]Department of Chemistry, Willard H. Dow Laboratories, University of Michigan, Ann Arbor, Michigan, 48109, USA.

[d]Institut de Chimie Moléculaire et des Matériaux d'Orsay, CNRS, Université de Paris-Sud 11, 91405 Orsay Cedex, France.

[e]CEA, Nuclear Energy Division, Radiochemistry Processes Department, DRCP, BP 17171, F-30207 Bagnols sur Cèze, France.

[b]Laboratoire de Chimie et Physique Quantiques, CNRS, Université Toulouse III, 118 route de Narbonne, 31062 Toulouse, France.

[f]e-mail address: bolvin@irsamc.ups-tlse.fr

S1 AILFT method

This method was developed by Atanasov, in a first time with Daul using DFT calculations [1] then with Neese for WFT [2]. The SO-CASSCF calculations provide the energies E_I and wave functions Ψ_I^{AI} of all the M states arising from the $4f^N$ configuration. They are developed as

$$\Psi_I^{AI} = \sum_{J=1}^{M} C_{IJ}\Phi_J \tag{S1}$$

with Φ_J a Slater determinant with N occupied f orbitals. The Hamiltonian matrix $\mathbf{H}^{AI}$ is built in the basis of the Φ_J expressed in terms of the real $4f$ orbitals. Since the *ab initio* $4f$ orbitals are close to pure metallic $4f$ orbitals, the correspondence with their model counter-part is easily performed. The model Hamiltonian of Eq. 1 depends on the parameters p_i, (i) the Slater-Condon parameters for electron-electron repulsion F^2, F^4 and F^6, (ii) the 28 CFPs associated to f orbitals, i.e. one parameter for each independent ligand field matrix elements $\langle f_m \left|\hat{v}_{CF}\right| f_{m'}\rangle$. Its matrix $\mathbf{H}^{LFT}(p_i)$ is expressed in the same basis of Slater determinants as the electronic structure calculations. The correspondence element by element of the two matrices leads to the equations to be solved. The problem is by far over-determined, but all equations are linear in the unknowns.

Those $M(M-1)/2$ equations arise from $\mathbf{H}^{LFT}(p_i) = \mathbf{H}^{AI}$ (AI stand for *ab initio*) and may be written in the form

$$\mathbf{A}\boldsymbol{P} = \mathbf{Y} \tag{S2}$$

where $\boldsymbol{P} = \{p_i\}$ .The parameter vector $\boldsymbol{P}$ is then determined by a least-square procedure according to

$$\boldsymbol{P} = \left(\mathbf{A}^\dagger\mathbf{A}\right)^{-1}\mathbf{A}^\dagger\mathbf{Y} \tag{S3}$$

S2 ITO method

S2.1 ITO decomposition

This method was developed by Ungur and Chibotaru [3]. A J manifold of the free ion is considered with wave-functions $\{|\Psi_I\rangle\}$ $(I = 1, 2J+1)$ and energies $\{E_I\}$, calculated with a CAS based method, in this work SO-CASSCF. This supposes that this manifold is well separated from the other ones and easily identifiable. In a first step, the $2J+1$ states must be assigned to the $\{|J,M\rangle\}$ $(M = -J, J)$ kets of the model space. Contrary to the AILFT method where the correspondence is performed at the orbital level, the assignment is done for the many-electron states and is specific to a J manifold. Noting that the $\{|J,M\rangle\}$ kets are innately eigenvectors of the Z component of the total angular momentum operator $\hat{J}_Z$, and according to Wigner-Eckart theorem, of the Z component of the magnetic moment $\hat{M}_Z$. Consequently, diagonalizing the matrix representation of $\hat{M}_Z$ in the set of the $\{|\Psi_I\rangle\}$ provides eigenvectors $\left\{\left|\widetilde{\Psi}_M\right\rangle\right\}$ which are the *ab initio* counterparts of the model $\{|J,M\rangle\}$. This is true towards a phase factor. In the model space, the relative phase factors of $|J,M\rangle$ and $|J,M\pm1\rangle$ are fixed by applying the ladder operators $\hat{J}_\pm$. It follows that the matrix representations of $\hat{M}_X$ and $\hat{M}_Y$ in the $|J,M\rangle$ are respectively real and pure imaginary. They are furthermore tridiagonal with a zero main diagonal. The phase factors of the $\left\{\left|\widetilde{\Psi}_M\right\rangle\right\}$ are chosen such that the upper diagonal of the $\hat{M}_X$ matrix becomes real. As a consequence, the upper diagonal of the $\hat{M}_Y$ matrix is almost pure imaginary. Finally, the Hamiltonian matrix $\mathbf{H}^{AI}$ (AI stands for *ab initio*), which is diagonal in the original set $\{|\Psi_I\rangle\}$, is expressed in the $\left\{\left|\widetilde{\Psi}_M\right\rangle\right\}$ basis. $\mathbf{H}^{AI}$ is the matrix to be decomposed in terms of irreducible tensors operators (ITOs) in order to obtain the CFPs.

The correspondence between the *ab initio* $\left\{\left|\widetilde{\Psi}_M\right\rangle\right\}$ and the model $\{|J,M\rangle\}$ is based on the similarity between the $\mathbf{M}_u^{AI}$ $(u=X,Y,Z)$ matrix representations of $\hat{\boldsymbol{M}}$ in the $\left\{\left|\widetilde{\Psi}_M\right\rangle\right\}$ basis and the $\mathbf{M}_u^J$, matrices of $g_J\hat{\boldsymbol{J}}$ in the $\{|J,M\rangle\}$ basis, where g_J is the Landé factor of the free ion. This similarity is quantified by the distance between those matrices as

$$\delta m_u = \sqrt{\mathrm{Tr}\left(\mathbf{M}_u^J - \mathbf{M}_u^{AI}\right)^\dagger \left(\mathbf{M}_u^J - \mathbf{M}_u^{AI}\right)} \tag{S4}$$

$\dagger$ denotes the conjugate transpose. δm_u vanishes in the limit of the free ion in the LS coupling scheme.

Matrix $\mathbf{H}^{AI}$ is now expanded in spin matrices $\mathbf{\Omega}_q^{(k)}$ of the ITOs $O_q^{(k)}$ in the basis $\{|J,M\rangle\}$ [4, 5]

$$\mathbf{H}^{AI} = \sum_{k=0}^{2J}\sum_{q=-k}^{k}(-1)^q Q_q^{(k)}\mathbf{\Omega}_{-q}^{(k)} \tag{S5}$$

The expansion coefficients are obtained by orthogonal projection

$$Q_q^{(k)} = \frac{2k+1}{\left|\left\langle J\left\|O^{(k)}\right\|J\right\rangle\right|^2}(-1)^q\,\mathrm{Tr}\left(\mathbf{\Omega}_{-q}^{(k)\dagger}\mathbf{H}^{AI}\right) \tag{S6}$$

where $\left|\left\langle J\left\|O^{(k)}\right\|J\right\rangle\right|$ is a reduced matrix element. The normalization of Görller-Walrand [6] is applied with $Q_q^{(k)}=1$ for $\frac{\sqrt{4\pi}}{\sqrt{2k+1}}Y_{kq}$. The $Q_q^{(k)}$ equals the CFPs B_q^k by the multiplication factor α_J^k of Eq. 4. Eq. S5 leads to $(2J+1)^2$ coefficients $Q_q^{(k)}$, the size of matrix $\mathbf{H}^{AI}$. If $\mathbf{H}^{AI}$ is traceless, $Q_0^{(0)}$ is zero. Since the Hamiltonian is a time-even operator, the terms with odd values of k vanish, and the hermiticity of the Hamiltonian leads to $Q_{-q}^{(k)} = Q_q^{(k)*}$ (see Section S2.2). Even orders larger than 6 do not have any reason to vanish, but those components are found to be less than 1 cm^{-1}. The matrix limited to the 27 CFPs

$$\tilde{\mathbf{H}} = \sum_{k=2,4,6}\sum_{q=-k}^{k}(-1)^q Q_q^{(k)}\mathbf{S}_{-q}^{(k)} \tag{S7}$$

is compared to the original *ab initio* one $\mathbf{H}^{AI}$ by calculating the distance δh between those two matrices

$$\delta h = \sqrt{\mathrm{Tr}\left(\tilde{\mathbf{H}} - \mathbf{H}^{AI}\right)^\dagger\left(\tilde{\mathbf{H}} - \mathbf{H}^{AI}\right)} \tag{S8}$$

In all cases, δh is very small, which confirms the validity of CF theory for $4f$ orbitals.

S2.2 Symmetry of the decomposition

In order to discuss the symmetry of the spin matrices $\mathbf{\Omega}_q^{(k)}$ of the ITOs $O_q^{(k)}$ in the basis $\{|J,M\rangle\}$, two types of symmetries should be considered:

- with respect to the main diagonal, a matrix $\mathbf{M}$ is (T denotes the transpose)
  - symmetric ($\mathbb{S}$) if $\mathbf{M} = \mathbf{M}^T$
  - antisymmetric ($\mathbb{A}$) if $\mathbf{M} = -\mathbf{M}^T$
- with respect to the skew diagonal, a matrix $\mathbf{M}$ is, with $\mathbf{J}$ the exchange matrix
  - per-symmetric ($\mathcal{S}$) if $\mathbf{M}.\mathbf{J} = \mathbf{J}.\mathbf{M}^T$

– per-antisymmetric ($\mathcal{A}$) if $\mathbf{M}.\mathbf{J} = -\mathbf{J}.\mathbf{M}^T$

Matrices $\mathbf{\Omega}_q^{(k)}$ fulfill the following properties

- for $q \neq 0$, $\mathbf{\Omega}_q^{(k)} + \left(\mathbf{\Omega}_q^{(k)}\right)^T$ is $\mathbb{S}$
- for $q \neq 0$, $\mathbf{\Omega}_q^{(k)} - \left(\mathbf{\Omega}_q^{(k)}\right)^T$ is $\mathbb{A}$
- for $k+q$ even, $\mathbf{\Omega}_q^{(k)}$ is $\mathcal{S}$
- for $k+q$ odd, $\mathbf{\Omega}_q^{(k)}$ is $\mathcal{A}$

The two last lines are easily shown by recursion since $\mathbf{\Omega}_0^{(0)}$, $\mathbf{\Omega}_{\pm 1}^{(1)}$ are $\mathcal{S}$ and $\mathbf{\Omega}_0^{(1)}$ is $\mathcal{A}$ and

$$O_q^{(k)} = N_k (-1)^q \sum_{q'=-1}^{1} \begin{pmatrix} k-1 & 1 & k \\ q-q' & q' & -q \end{pmatrix} O_{q-q'}^{(k-1)} O_{q'}^{(1)} \tag{S9}$$

Matrix $\mathbf{H}^{AI}$ is Hermitian and is the representation matrix of a even-time operator. The first property implies that for $q \neq 0$

$$\begin{aligned} \mathrm{Im}\left[\mathbf{\Omega}_q^{(k)} + \left(\mathbf{\Omega}_q^{(k)}\right)^T\right] &= 0 \\ \mathrm{Re}\left[\mathbf{\Omega}_q^{(k)} - \left(\mathbf{\Omega}_q^{(k)}\right)^T\right] &= 0 \end{aligned} \tag{S10}$$

The basis set in which $\mathbf{H}^{AI}$ is developed is the *ab initio* counterpart of the $\{|J, M\rangle\}$ basis, which behaves under time inversion $\mathcal{K}$ as

$$\mathcal{K}\,|J, M\rangle = (-1)^{J-M+n}\,|J, -M\rangle \tag{S11}$$

where n is the sum of the orbital quantum numbers of all the electrons in the atom [7]. It follows that

$$\mathcal{K}\left\langle J, M \left|\hat{\mathcal{H}}\right| J, M'\right\rangle = (-1)^{-M-M'}\left\langle J, -M' \left|\hat{\mathcal{H}}\right| J, -M\right\rangle \tag{S12}$$

The per-symmetry connects $(M, M') \longleftrightarrow (-M', -M)$. In other words, Eq. S12 means that the elements of $\mathbf{H}^{AI}$ with $q = M - M'$ even (odd) are $\mathcal{S}$ ($\mathcal{A}$). Matrices $\mathbf{\Omega}_q^{(k)}$ have only non zero elements on the qth diagonal below ($q > 0$) or above ($q < 0$) the skew-diagonal. In the case of odd k, $\mathbf{\Omega}_q^{(k)}$ is $\mathcal{S}$ for odd q, and $\mathcal{A}$ for even q. Hence, the $\mathbf{\Omega}_q^{(k)}$ matrices with odd k are orthogonal to $\mathbf{H}^{AI}$, and do not contribute to the ITO expansion.

In terms of CFPs, due to their imaginary character, each B_q^k is in principle described by two degrees of freedom. However, because of Eqs. S10 arising from the hermiticity of the Hamiltonian, the four degrees of freedom of B_q^k and B_{-q}^k reduce to two: $\mathrm{Re}B_q^k = \pm \mathrm{Re}B_{-q}^k$ and $\mathrm{Im}B_q^k = \pm \mathrm{Im}B_{-q}^k$. Furthermore, due to time inversion symmetry, all B_q^k with odd k vanish. It should be mentioned that it only holds if the condition that phase factors are appropriately chosen, as proposed in Section S2.1. Finally, k orders larger than 6 are found negligible (less than 10^{-4} cm^{-1}). This does not arise from symmetry reasons but from the relevance of the LS coupling scheme in $4f$ elements, as seen from how small δm_u are (see Eq. S4 and Tables S1 and S4).

S3 $LnZn_{16}$ series

Table S1: CFPs (cm^{-1}) in the $LnZn_{16}$ series, δm_u (μ_B) and δh (cm^{-1}) distances between *ab initio* and model matrices (see Eqs. S4 and S8).

	FIT			ITO											
Ln	B_0^2	B_0^4	B_0^6	B_0^2	B_0^4	B_0^6	B_1^2	B_2^2	B_4^4	B_4^6	B_6^6	δm_x	δm_y	δm_z	δh
Tb	-1163	-623	1169	-1162	-620	1182	0	0	12	29	0	0.34	0.34	0.36	10
Dy	-1111	-694	684	-1112	-692	685	0	0	10	8	0	0.24	0.24	0.10	7
Ho[Dy][a]	-1069	-587	565	-1068	-586	564	0	2	4	7	3	0.19	0.19	0.18	4.5
Ho[Er][b]	-955	-652	577	-954	-652	577	0	5	14	9	0	0.19	0.19	0.18	5.4
Er	-958	-669	568	-958	-669	567	0	11	24	19	10	0.09	0.09	0.12	5.8
Yb	-958	-495	438	-958	-495	438	0	2	12	7	2	0.02	0.02	0.03	0

a: with the structure of $DyZn_{16}$. *b*: with the structure of $ErZn_{16}$.

Table S2: Energy (cm^{-1}) and $|M_J|$ in parenthesis of the ground J manifold of $LnZn_{16}$ calculated with SO-CASSCF.

state		1	2	3	4	5	6	7	8	9	10	11	12	13	14	15	16	17
Tb	E	0	19	19	75	83	189	189	353	353	541	541	589	589				
	$\|M_J\|$	*0*	*1*	*1*	*2*	*2*	*3*	*3*	*4*	*4*	*5*	*5*	*6*	*6*				
Dy	E	0.0		32		84		135		174		216		329		704		
	$\|M_J\|$	*1/2*		*3/2*		5/2		*7/2*		9/2		11/2		13/2		*15/2*		
Ho[Dy][a]	E	0	1	17	19	55	55	76	78	136	137	161	183	183	263	263	317	317
	$\|M_J\|$	*4*	*4*	*3*	*3*	*5*	*5*	*2*	*2*	*1*	*1*	*0*	*6*	*6*	*8*	*8*	*7*	*7*
Ho[Er][b]	E	0	1	23	23	50	51	87	89	151	152	176	176	177	253	253	310	310
	$\|M_J\|$	*4*	*4*	*3*	*3*	*5*	*5*	*2*	*2*	*1*	*1*	*6*	*6*	*0*	*8*	*8*	*7*	*7*
Er	E	0		53		134		150		190		269		284		320		
	$\|M_J\|$	*13/2*		*15/2*		*1/2*		*11/2*		3*/2*		*5/2*		*9/2*		*7/2*		
Yb	E	0		87		397		494										
	$\|M_J\|$	*7/2*		*5/2*		*3/2*		*1/2*										

a: with the structure of $DyZn_{16}$. *b*: with the structure of $ErZn_{16}$.

S4 $[Ln(DPA)_3]^{3-}$ series

S4.1 *Ab initio* results

Table S3: Energy (cm^{-1}) of the first excited states of $[Ln(DPA)_3]^{3-}$calculated with SO-CASSCF M: MOLCAS, O: ORCA. J for the ground state is given. Different J manifolds are separated by a vertical line.

Ln	J		E_1	E_2	E_3	E_4	E_5	E_6	E_7	E_8	E_9	E_{10}	E_{11}	E_{12}	E_{13}	E_{14}	E_{15}	E_{16}	E_{17}
Ce	5/2	M	0	0	348	348	389	389	2327	2327	2639	2639	2805	2805	2914	2914			
		O	0	0	349	349	391	391	2311	2311	2615	2615	2787	2787	2894	2894			
Pr	4	M	0	18	43	68	144	152	254	315	471								
		O	0	20	47	74	145	156	261	320	476								
Nd	9/2	M	0	0	48	48	155	155	300	300	374	374							
		O	0	0	46	46	157	157	298	298	369	369							
Sm	5/2	M	0	0	74	74	120	120	1035	1035	1081	1081	1176	1176	1255	1255			
		O	0	0	74	74	125	125	1029	1029	1070	1070	1161	1161	1239	1239			
Eu	0	M	0	340	367	415	1014	1034	1079	1105	1130	1958	1993	2002	2005	2025	2046	2052	
		O	0	334	360	412	976	994	1037	1063	1084	1856	1888	1896	1901	1918	1939	1944	
Tb	6	M	0	1	53	58	68	89	93	171	175	189	189	207	209				
		O	0	0	65	70	82	103	108	183	187	202	205	218	220				
Dy	15/2	M	0	0	19	19	40	40	60	60	99	99	158	158	211	211	261	261	
		O	0	0	20	20	39	39	55	55	94	94	161	161	215	215	265	265	
Ho	8	M	0	6	7	53	65	92	113	117	128	179	184	212	270	272	284	296	297
		O	0	6	8	53	64	89	112	116	127	176	180	210	265	266	280	292	293
Er	15/2	M	0	0	20	20	99	99	130	130	181	181	241	241	268	268	324	324	
		O	0	0	22	22	99	99	131	131	182	182	242	242	268	268	324	324	
Tm	6	M	0	18	53	104	126	171	194	200	231	239	261	267	286				
		O	0	18	55	108	127	172	200	205	241	249	262	275	292				
Yb	7/2	M	0	0	42	42	118	118	228	228									
		O	0	0	41	41	117	117	232	232									

Table S4: δm_u (μ_B) and δh (cm^{-1}) distances between *ab initio* and model matrices (see Eqs. S4 and S8) for the $[Ln(DPA)_3]^{3-}$ series.

Ln	J	g_J	δm_x	δm_y	δm_z	δh
Ce	5/2	6/7	0.30	0.30	0.23	0
Pr	4	4/5	0.30	0.28	0.17	18
Nd	9/2	8/11	0.51	0.48	0.18	36
Sm	5/2	2/7	0.55	0.60	0.28	0
Tb	6	3/2	0.23	0.25	0.17	3
Dy	15/2	4/3	0.24	0.22	0.19	6
Ho	8	5/4	0.22	0.21	0.18	3
Er	15/2	6/5	0.13	0.13	0.09	2
Tm	6	7/6	0.06	0.06	0.04	3
Yb	7/2	8/7	0.03	0.03	0.02	0

Table S5: g factors of the ground Kramers doublet for the $[Ln(DPA)_3]^{3-}$ series with odd number of electrons. $Z_{\parallel}$ is the principal axis of the **g** tensor with smallest angle α (°) with Z axis (see Fig. S1). $\omega^{Z}_{M_J}$ and $\omega^{g_{max}}_{M_J}$ are the weights of the wave function on component M_J with quantification axis Z and the principal direction of the largest g, respectively (the largest weight is given).

	$g_\perp$	$g_\perp$	$g_\parallel$	α	$\omega^{Z}_{M_J}$ (M_J)	$\omega^{g_{max}}_{M_J}$ (M_J)
Ce	0.9	0.4	2.2	7	0.64 (5/2)	0.64 (5/2)
Nd	3.0	2.6	1.9	48	0.62 (7/2)	0.52 (5/2)
Sm	0.1	0.8	0.2	35	0.79 (1/2)	0.65 (5/2)
Dy	4.3	1.0	14.6	42	0.49 (9/2)	0.53 (15/2)
Er	3.7	12.5	1.6	6	0.47 (7/2)	0.28 (15/2)
Yb	2.4	6.1	1.2	31	0.47 (3/2)	0.79 (7/2)

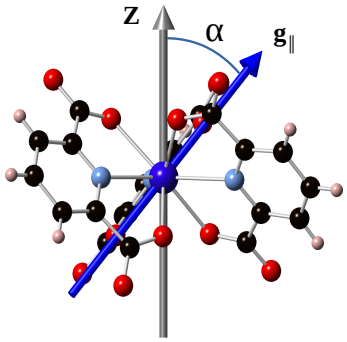

Figure S1: Z axis and principal axis corresponding to $g_{\parallel}$ for the $DyZn_{16}$ complex.

Table S6: CFPs (in cm^{-1}) in the $[Ln(DPA)_3]^{3-}$ series calculated with AILFT.

Ln	B^2_0	$\tilde{B}^2_1$	$\tilde{B}^2_2$	B^4_0	$\tilde{B}^4_1$	$\tilde{B}^4_2$	$\tilde{B}^4_3$	$\tilde{B}^4_4$	B^6_0	$\tilde{B}^6_1$	$\tilde{B}^6_2$	$\tilde{B}^6_3$	$\tilde{B}^6_4$	$\tilde{B}^6_5$	$\tilde{B}^6_6$
Ce	282	78	62	-740	35	52	941	48	-510	15	113	789	40	120	889
Pr	278	70	69	-672	31	55	823	37	-513	13	98	710	33	95	856
Nd	265	79	60	-589	23	48	699	34	-478	13	85	627	19	89	779
Sm	240	83	56	-471	17	43	525	31	-403	14	67	487	18	71	649
Eu	239	85	54	-427	18	38	466	29	-380	15	60	442	17	65	599
Tb	223	76	50	-351	11	41	363	21	-335	12	49	358	20	49	522
Dy	234	81	54	-325	13	38	328	22	-327	12	47	333	20	47	496
Ho	236	79	49	-294	10	31	289	19	-310	11	40	301	19	39	460
Er	238	75	44	-272	10	31	260	17	-296	12	38	276	17	36	435
Tm	236	85	54	-251	11	31	233	18	-278	12	36	253	20	36	409
Yb	230	87	50	-239	9	27	213	18	-266	12	32	232	19	30	392

Table S7: CFPs (in cm^{-1}) in the $[Ln(DPA)_3]^{3-}$ series calculated with ITO.

Ln	B_0^2	$\bar{B}_1^2$	$\bar{B}_2^2$	B_0^4	$\bar{B}_1^4$	$\bar{B}_2^4$	$\bar{B}_3^4$	$\bar{B}_4^4$	B_0^6	$\bar{B}_1^6$	$\bar{B}_2^6$	$\bar{B}_3^6$	$\bar{B}_4^6$	$\bar{B}_5^6$	$\bar{B}_6^6$
Ce	276	66	61	-720	26	75	985	71	-687	30	94	897	10	107	838
Pr	206	67	58	-648	41	69	749	31	-523	29	88	662	43	88	774
Nd	123	90	59	-540	22	39	524	17	-423	32	75	602	48	98	733
Sm	217	58	79	-260	45	60	477	99	-362	22	76	412	31	64	636
Eu	240	71	36	-206	10	86	457	38	-491	35	60	335	42	86	490
Tb	223	77	54	-445	16	50	456	13	-471	45	33	397	27	47	628
Dy	207	83	55	-414	8	47	362	31	-340	25	49	337	31	50	546
Ho	211	82	51	-317	7	29	287	20	-327	21	43	317	28	44	500
Er	265	76	41	-319	12	43	317	44	-331	10	43	290	13	36	461
Tm	223	90	57	-258	3	31	249	24	-278	21	38	264	28	41	437
Yb	210	90	52	-251	3	27	222	17	-274	19	36	238	29	35	394

Table S8: Strength parameters (in cm^{-1}) in the $[Ln(DPA)_3]^{3-}$ series calculated with AILFT.

Ln	S	S^2	S^4	S^6	S_0	S_1	S_2	S_3	S_4	S_5	S_6
Ce	417	141	509	492	311	52	64	541	27	47	349
Pr	381	139	449	462	293	47	63	478	22	37	336
Nd	337	134	385	417	265	51	55	411	18	35	306
Sm	269	124	294	340	221	53	49	313	16	28	255
Eu	247	124	263	312	207	55	45	280	15	25	235
Tb	206	115	209	267	180	48	42	221	13	19	205
Dy	195	121	190	253	176	52	43	202	13	18	194
Ho	180	121	169	233	168	50	38	180	11	15	180
Er	169	120	154	219	162	48	35	164	11	14	171
Tm	160	123	139	205	155	54	40	148	11	14	160
Yb	152	121	129	194	150	55	36	135	11	12	154

Table S9: Strength parameters (in cm^{-1}) in the $[Ln(DPA)_3]^{3-}$ series calculated with ITO.

Ln	S	S^2	S^4	S^6	S_0	S_1	S_2	S_3	S_4	S_5	S_6
Ce	434	136	525	521	330	45	64	583	34	42	329
Pr	350	108	416	428	276	48	60	438	22	35	304
Nd	292	88	306	394	222	59	51	342	20	38	288
Sm	241	115	248	316	164	43	65	277	48	25	249
Eu	218	119	230	274	186	47	52	252	24	34	192
Tb	249	116	262	321	221	52	43	265	12	18	246
Dy	212	112	221	271	191	54	46	216	19	20	214
Ho	187	112	173	251	168	53	39	184	14	17	196
Er	188	130	186	234	184	49	37	188	21	14	181
Tm	166	120	147	216	153	58	42	157	16	16	171
Yb	153	115	135	197	147	57	38	140	14	14	155

S4.2 Minor CFPs

Figures S2 represent the CFPs of Tables S6 and S7 with $q = 1, 2, 4, 5$ and the corresponding strength parameters S_q of Tables S8 and S9. All those parameters are less than 100 cm^{-1}, in accordance with the pseudo ternary symmetry of the complexes.

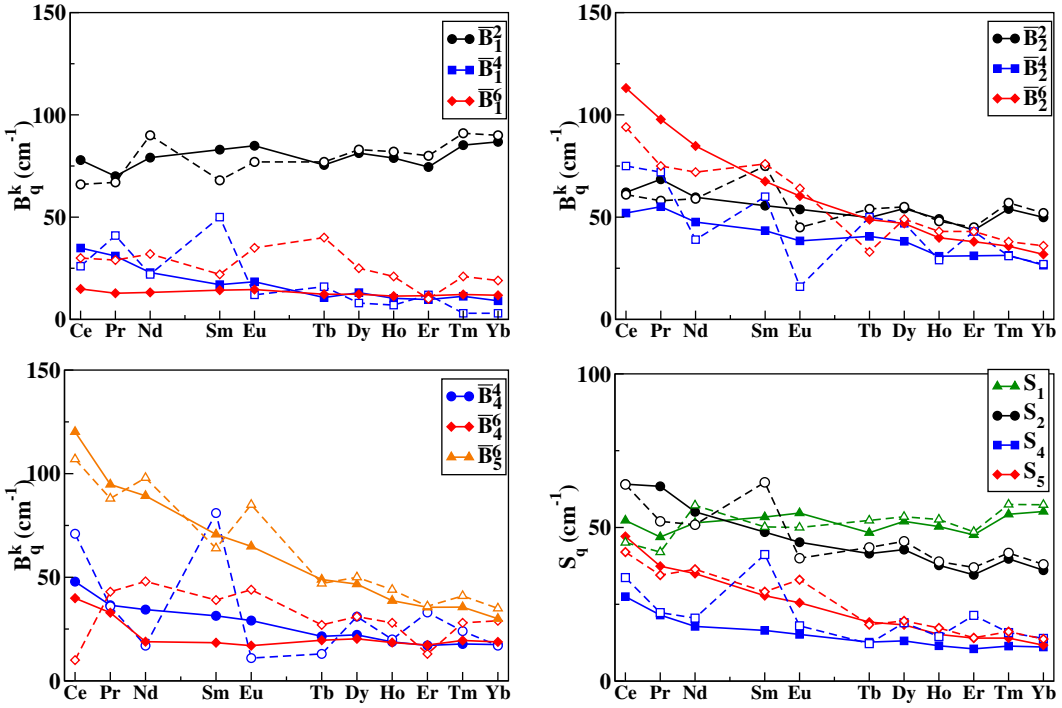

Figure S2: CFPs and strength parameters (cm^{-1}) in the $[Ln(DPA)_3]^{3-}$ series. Solid line: AILFT full spectrum; Dashed line: ITO.

S4.3 Two electron parameters

Figure S3 represent the Slater-Condon parameters in the series. The parameters increase in the series since the $4f$ orbitals become more compact as it usually the case [8, 9].

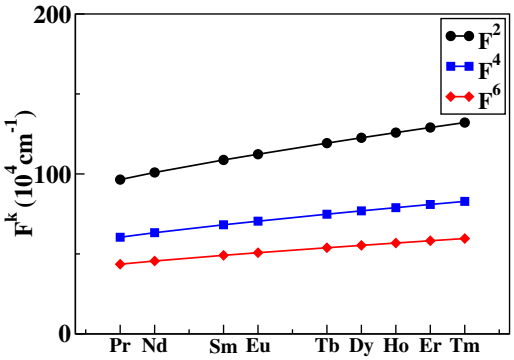

Figure S3: Slater-Condon parameters (cm^{-1}) in the $[Ln(DPA)_3]^{3-}$ series.

S4.4 $J - J$ coupling and CFPs

Comparison of the CFPs (Fig. 4) and strength parameters (Fig. 5) deduced with AILFT and ITO show that in the first half of the series they are smaller with the latter method and the opposite occurs in the second half of the series. With AILFT, the CFPs are extracted at orbital level and the other effects are described by specific parameters, the spin-orbit coupling by the ζ parameter and the two-electron interactions by the Slater-Condon parameters depicted in Figure S3. With ITO, the CFPs include all the effects in an effective way. Spin-orbit coupling leads to

the so called $J-J$ coupling in the free ion, by mixing LS terms with the same value of J. This impacts strongly the energies of the first half of the series, and specially the energies of the states arising from excited J manifold in Table S3. In order to quantify the effect of the $J-J$ coupling on the CFPs, they are deduced from the ground L manifold: the procedure described in Section S2.1 is applied by replacing J by L and in Eq. 4 α_J^k is replaced by α_L^k [10]. Strength parameters deduced from L and J ground manifolds are compared in Figures S4 ; the small discrepancies are meaningless. It shows that i) the $J-J$ coupling affects the energetic spectrum by moving a whole J manifold, but does not affect the splitting itself, and consequently, does not affect the CFPs. ii) the difference between the CFPs calculated with AILFT and ITO must be due to the many electron terms since they included in an effective way in the latter. In reference [10], it was shown that the composition of the many electron wave function of the complex was broadly the one of the free ion, but due to the splitting of the $4f$ orbitals by the ligands, there are small variations that might affect the effective CFPs.

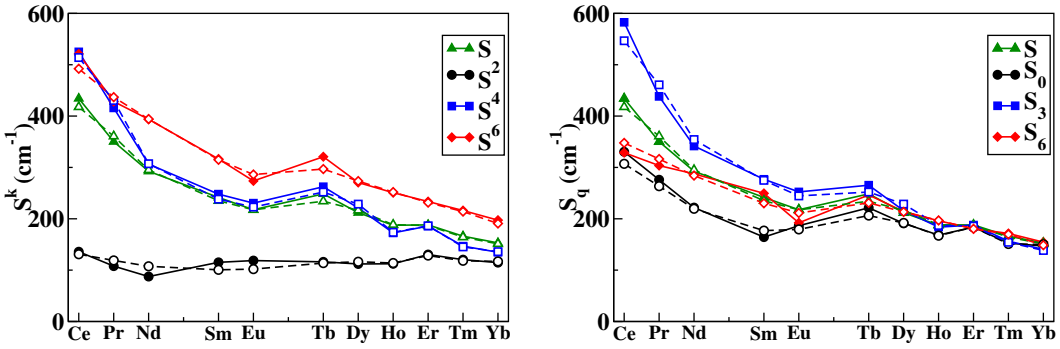

Figure S4: Strength parameters (cm^{-1}) in the $[Ln(DPA)_3]^{3-}$ series calculated from the ground J (plain line) and the L (dashed line) manifolds.

S4.5 CFPs from point charges model

In reference [10], the covalent contributions to CFPs were determined as the difference between *ab initio* and a point charges (PC) model. In this PC model, the ligands are replaced by point charges (PCs) reproducing the multipoles of the ligands. It was shown that these contributions affect the CFPs, both qualitatively and quantitatively. For the $[Ln(DPA)_3]^{3-}$ complexes, the PC model is built as follow: each atom (including hydrogens) is replaced by a PC according to its LoProp charge value [11]. The dipole and quadrupole moments of the complex obtained with this PC model were larger than those of the *ab initio* complex. A multiplicative factor of 0.9 has been applied to each charge in order to be closer than the *ab initio* potential and then, as shown in Table S10, the PC model reproduces well the electrostatic potential of the 'real' ligands. In this model, the lanthanide ion is described by a basis set, such those calculations take into account the screening of the $4f$ orbitals by the filled $5s5p$ orbitals and the polarization of the metal orbitals by the field of the ligands. The strength parameters calculated with this PC model are shown in Figure 7 and compared to the full molecule values. This figure is discussed in the main article. A simplified PC model has been considered: only the coordinating oxygen and nitrogen atoms are considered and are replaced by PCs Q^0 = -0.85 and Q^N = -0.3 respectively, based on their LoProp charge. This simplified PC model gives rise to dipole and quadrupole moments rather different from the previous ones. Strength parameters are compared for the two PC models on Figure S6. The results are rather similar, except S^4 and S_3 which are larger with simplified PC model, but with similar trends.

Table S10: Dipole (D) and quadrupole (D.Å) moments of the $LnZn_{16}$series, full *ab initio* (AI) and with the point charge model (PC).

Ln		d_X	d_Y	d_Z	Q_{XX}	Q_{XY}	Q_{XZ}	Q_{YY}	Q_{YZ}	Q_{ZZ}
Ce	AI	1.55	1.22	-1.01	17.11	-5.48	3.00	42.02	4.68	-59.13
	PC	1.42	1.30	-1.10	19.05	-5.08	2.77	43.38	4.70	-62.43
Pr	AI	-1.02	1.10	0.88	19.37	7.81	4.25	41.21	-4.39	-60.58
	PC	-0.85	1.17	0.98	20.83	7.73	4.21	42.04	-4.43	-62.87
Nd	AI	-1.05	1.41	0.74	19.90	7.90	4.49	41.08	-3.80	-60.98
	PC	-0.90	1.48	0.81	21.50	7.65	4.24	42.00	-3.84	-63.51
Sm	AI	-0.92	1.46	0.63	20.94	7.75	4.26	41.07	-3.70	-62.02
	PC	-0.75	1.53	0.71	22.50	7.48	4.00	42.04	-3.85	-64.54
Eu	AI	-0.99	1.55	0.63	21.17	7.15	3.88	41.30	-3.45	-62.48
	PC	-0.85	1.60	0.70	23.16	6.97	3.77	41.93	-3.72	-65.08
Tb	AI	0.96	1.28	-0.57	20.12	-3.82	2.66	42.77	4.08	-62.90
	PC	0.79	1.38	-0.67	21.76	-3.74	2.36	43.76	4.23	-65.52
Dy	AI	-0.91	1.42	0.58	21.90	6.67	4.03	41.42	-3.83	-63.31
	PC	-0.75	1.50	0.66	23.39	6.45	3.81	42.38	-3.94	-65.77
Ho	AI	-0.76	1.40	0.52	22.32	6.38	3.84	41.30	-3.57	-63.62
	PC	-0.59	1.46	0.61	23.88	6.20	3.61	42.46	-3.67	-66.34
Er	AI	0.94	1.31	-0.37	21.01	-3.08	2.85	41.99	3.90	-63.00
	PC	0.77	1.40	-0.44	22.76	-3.04	2.52	43.02	4.08	-65.78
Tm	AI	-0.87	1.45	0.54	22.50	5.97	3.90	41.35	-3.31	-63.84
	PC	-0.69	1.51	0.63	24.11	5.83	3.65	42.57	-3.52	-66.68
Yb	AI	-0.80	1.42	0.51	22.97	5.79	3.77	40.87	-3.73	-63.84
	PC	-0.62	1.51	0.59	24.67	5.78	3.35	42.15	-3.85	-66.82

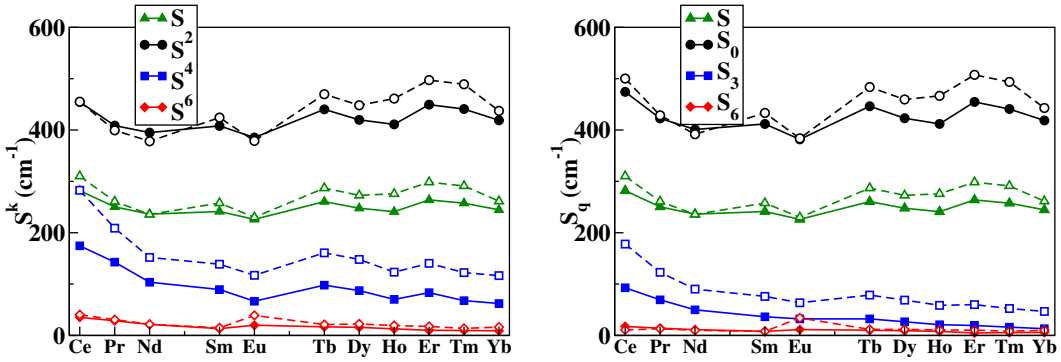

Figure S5: Strength parameters (cm^{-1}) in the $[Ln(DPA)_3]^{3-}$ series. Full line: PC model, dashed line: simplified PC model.

With the PC models, the strength parameters are rather constant in the series. Since both the nature of the metal ion and the position of the point charges change along the series, one expects two opposite trends. On one hand, the metal-ligand bond shrinks, increasing the electrostatic interactions and consequently the CFPs. On the other hand, the radial expansion of the $4f$ orbitals decreases, and this reduces the interactions, and the CFPs. In order to unravel those two effects, the nature of the ion and the compression of the coordination sphere were varied independently. In Figure S8, the distances are varied and the metal atom is kept the same, and in Figure S7, the metal is varied in a constant environment. S increases by 30% in the former case, and decreases by 30 % in the latter, more irregularly. The combined effects lead to rather constant CFPs across the series.

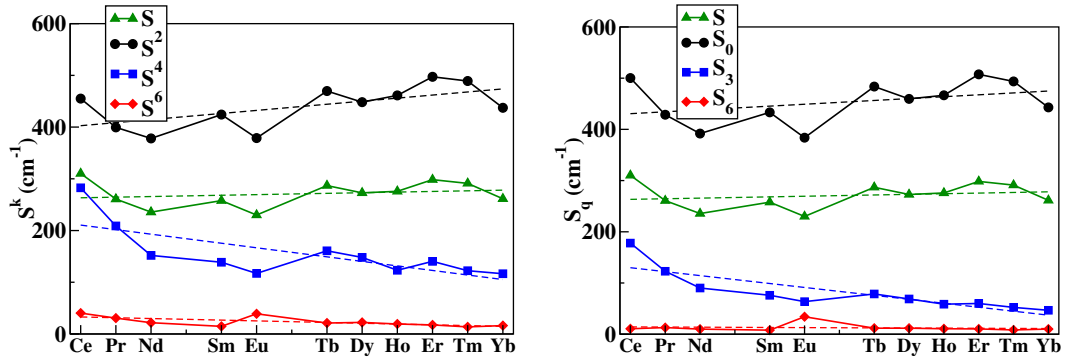

Figure S6: Strength parameters (cm^{-1}) in the $[Ln(DPA)_3]^{3-}$ series obtained with the simplified PC model. Linear regression lines are indicated as dashed lines.

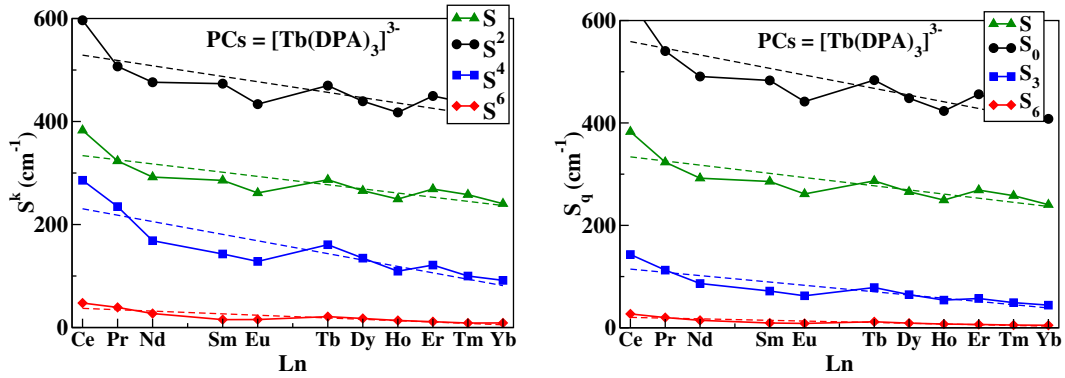

Figure S7: Strength parameters (cm^{-1}) in the $[Ln(DPA)_3]^{3-}$ series obtained with the simplified PC model keeping the position of the charges fixed. Linear regression lines are indicated as dashed lines.

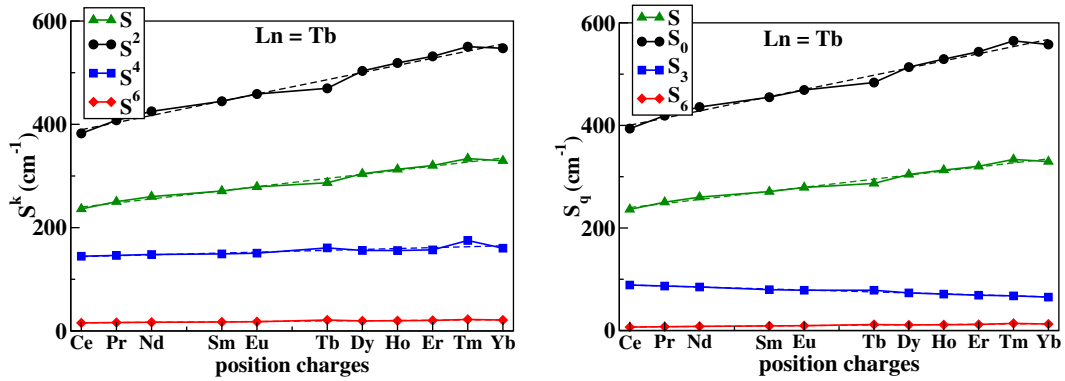

Figure S8: Strength parameters (cm^{-1}) in the $[Ln(DPA)_3]^{3-}$ series obtained with the simplified PC model keeping the lanthanide ion fixed. Linear regression lines are indicated as dashed lines.

S4.6 B_q^k from pNMR shifts

In reference [12], B_0^2 was determined in the $[Ln(DPA)_3]^{3-}$ series, towards an arbitrary factor, from ^{13}C and ^{1}H pNMR shifts by applying Bleaney's theory. In this model, the CF of the ligands is reduced to only B_0^2 and is considered as constant in the Ln series. The aim of this Section is

to convert the value of B_0^2 found in reference [12] from arbitrary units to cm^{-1} using Wybourne normalization, in order to compare it to the present work.

In Bleaney's theory, the paramagnetic shift of a nucleus i, i.e. the fractional shift $\Delta\nu/\nu$ in a nuclear resonance frequency due the presence of the paramagnetic center, is (Eq. 19 of reference [13]) expressed with the international system of units,

$$\delta^{pc} = \frac{\Delta\nu}{\nu} = -\frac{\mu_0\mu_B^2}{4\pi * 60\,(k_BT)^2} * 2 * \left(g_J^2 J(J+1)(2J-1)(2J+3)\,\langle J\,\|\alpha\|\,J\rangle\right) * \frac{3\cos^2\theta - 1}{r^3} A_2^0 < r^2 > \quad \text{(S13)}$$

with μ_0 the magnetic constant, μ_B the Bohr magneton, k_B the Boltzmann constant, T the temperature, g_J the Landé term of the paramagnetic ion with J, L and S its total, orbital and spin electronic angular momenta. θ and r define the position of the nucleus i with respect to the paramagnetic center. $A_2^0 < r^2 >$ is the 2nd order CFP within Steven's notation. Eq. S13 is usually rewritten as follow

$$\delta^{pc} = G_i * A_2^0 < r^2 > C_a^D \quad \text{(S14)}$$

with

$$G_i = \frac{3\cos^2\theta - 1}{r^3} \quad \text{(S15)}$$

which depends only on the position of the nucleus of interest, and

$$C_a^D = -\frac{2\mu_0\mu_B^2}{4\pi * 60\,(k_BT)^2} X(J) \quad \text{(S16)}$$

with $X(J) = g_J^2 J(J+1)(2J-1)(2J+3)\,\langle J\,\|\alpha\|\,J\rangle$. C_a^D depends only on the nature of the lanthanide ion, and has been tabulated by Bleaney *et al.* [14] using arbitrary units with $\tilde{C}_{\mathrm{Dy}}^D = 100$ for Dy.

$X(J) =$ -181 for Dy(III) and using SI units, $C_{\mathrm{Dy}}^D = 3.06\,10^{-6}$ $m^3.J^{-1}$ at 298 K. If δ^{pc} is expressed in ppm, r in Å and $A_2^0 < r^2 >$ in cm^{-1}, $C_{\mathrm{Dy}}^D = 60$ $Å^3/cm^{-1}$. It follows that the values of $A_2^0 < r^2 >$ determined using the arbitrary value of C_a^D should be divided by a factor of 0.6 in order to get the value in in cm^{-1}. A further factor 2 is needed in order to get B_0^2 with Wybourne's convention. In reference [12], $A_2^0 < r^2 >$ was determined from Eq. S14 for the $[Ln(DPA)_3]^{3-}$ series to be 51. The corresponding value is $B_0^2 = 62$ cm^{-1}.

References

[1] Atanasov, M.; Daul, C. A.; Rauzy, C. A DFT based ligand field theory. In *Optical Spectra and Chemical Bonding in Inorganic Compounds: Special Volume dedicated to Professor Jørgensen I*; Mingos, D. M. P.; Schönherr, T., Eds.; Springer Berlin Heidelberg: Berlin, Heidelberg, 2004.

[2] Atanasov, M.; Aravena, D.; Suturina, E.; Bill, E.; Maganas, D.; Neese, F. First principles approach to the electronic structure, magnetic anisotropy and spin relaxation in mononuclear 3d-transition metal single molecule magnets. *Coord. Chem. Rev.* **2015**, *289*, 177.

[3] Ungur, L.; Chibotaru, L. F. Ab Initio crystal field for lanthanides. *Chem. Eur. J.* **2017**, *23*, 3708–3718.

[4] Zare, R. N. *Angular momentum;* Wiley: New-York, 1988.

[5] Van den Heuvel, W.; Soncini, A. NMR chemical shift as analytical derivative of the Helmholtz free energy. *J. Chem. Phys.* **2013**, *138*, 054113.

[6] Görller-Walrand, C.; Binnemans, K. Chapter 155 Rationalization of crystal-field parametrization. In *Handbook on the Physics and Chemistry of Rare Earths*, Vol. 23; Elsevier: , 1996.

[7] Barron, L. D.; Buckingham, A. D. Time reversal and molecular properties. *Acc. Chem. Res.* **2001**, *34*, 781–789.

[8] Duan, C.-K.; Tanner, P. A. What use are crystal field parameters? A chemist's viewpoint. *J. Phys. Chem. A* **2010**, *114*, 6055–6062.

[9] Jung, J.; Atanasov, M.; Neese, F. Ab Initio ligand-field theory analysis and covalency trends in actinide and lanthanide free ions and octahedral complexes. *Inorg. Chem.* **2017**, *56*, 8802–8816.

[10] Alessandri, R.; Zulfikri, H.; Autschbach, J.; Bolvin, H. Crystal field in rare-earth complexes: from electrostatics to bonding. *Chem. Eur. J.* **2018**, *24*, 5538–5550.

[11] Gagliardi, L.; Lindh, R.; Karlström, G. Local properties of quantum chemical systems: The LoProp approach.. *J. Chem. Phys.* **2004**, *121*, 4494–4500.

[12] Autillo, M.; Guerin, L.; Dumas, T.; Grigoriev, M. S.; Fedoseev, A. M.; Cammeli, S.; Solari, P. L.; Guilbaud, P.; Moisy, P.; Bolvin, H.; Berthon, C. Insight of the metal-ligand interaction in f elements complexes by paramagnetic NMR spectroscopy. *Chem. Eur. J.* **2019**, *25*, 4435.

[13] Bleaney, B. Nuclear magnetic resonance shifts in solution due to lanthanide ions. *J. Magn. Reson.* **1972**, *8*, 91.

[14] Bleaney, B.; Dobson, M.; Levine, B. A.; Martin, R. B.; Williams, R. J. P.; Xavier, A. V. Origin of lanthanide nuclear magnetic resonance shifts and their uses. *J. Chem. Soc. Chem. Comm.* **1972**, *13*, 791–793.